Inorganic Chemistry

Article

pubs.acs.org/IC

# Homoatomic Clustering in $T_4Ga_5$ (T = Ta, Nb, Ta/Mo): A Story of Reluctant Intermetallics Crystallizing in a New Binary Structure Type

Rie T. Fredrickson, Brandon J. Kilduff, and Daniel C. Fredrickson*

Department of Chemistry, University of Wisconsin—Madison, 1101 University Avenue, Madison, Wisconsin 53706, United States

Supporting Information

**ABSTRACT:** In the formation of binary compounds, heteroatomic interactions are generally expected to play the leading role in providing stability. In this Article, we present a series of gallides, $T_4Ga_5$ (T = Ta, Nb, and Ta/Mo), which appear to defy this expectation. Their complex crystal structures represent a new binary structure type (to the best of our knowledge),, which can be visualized in terms of a host lattice of T@$T_8$ body centered cubic (bcc) clusters linked through face-capping $Ga_2$ dumbbells to form a primitive cubic framework. The cubic spaces that result are alternately filled by distorted T pentagonal dodecahedra (sharing atoms with the host lattice) and dimers of bcc fragments, leading to a $\sqrt{2} \times \sqrt{2} \times 2$ supercell of the host framework structure. Ga tetrahedra and icosahedral units fill the remaining void spaces. Underlying these structural features is a strong tendency for homoatomic clustering of Ta and Ga, which is evident in all of the coordination polyhedra. Electronic structure calculations using density functional theory (DFT) and DFT-calibrated Hückel models reveal possible origins for this elemental segregation and the factors stabilizing the structure as a whole. A deep pseudogap is present at the Fermi energy of $Ta_4Ga_5$ (as well as at that of $Nb_4Ga_5$), corresponding to the near-optimization of Ta−Ta and Ta−Ga interactions. This pseudogap emerges as a result of the ability of extensive Ta−Ta bonding to provide local 18-electron configurations to the Ta atoms, despite the electron concentration being only 8.75 electrons per Ta atom. Support for these Ta−Ta interactions is provided by Ga bridging atoms, whose valence orbitals' low number of angular nodes confers preferential stabilization to Ta−Ta bonding functions over antibonding ones. The observed spatial separation of the structure into Ta and Ga domains occurs as a consequence of the Ga atoms being pushed toward the periphery of the Ta clusters to play this supporting role.

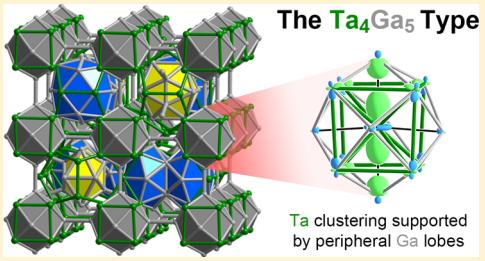


## 1. INTRODUCTION

The theme of "like dissolves like" in solubility and intermolecular interactions has some curious extensions into the realm of metallic phases. Certain combinations of metals refuse to be alloyed together to form solid solutions and in some cases will form two-phase liquids in the melt.[1] In intermetallic phases, this theme can be perceived in some of the most complex crystal structures, where large unit cells arise from segregation of the atoms into domains of differing polarity,[2] packing types,[3−5] or groupings of elements.[6−9] For most of these cases, the driving forces holding the conflicting domains together remain a matter of speculation, but if understood, they could offer new avenues to guiding the crystal structures of metallic materials. In this Article, we describe a series of transition metal gallides—$Ta_4Ga_5$, $Nb_4Ga_5$, and $Ta_{3.9}Mo_{0.1}Ga_5$—that illustrate one mechanism by which such segregation can occur in intermetallics.

Our first encounter with this series occurred during syntheses in the Mo−Ga system, which were inspired by the host−guest arrangements exhibited by the structures of $Mo_6Ga_{31}$[10] and the $V_8Ga_{41}$-type[11,12] phase $Mo_8Ga_{41}$,[13] and the prospect of a larger progression of structures based on these motifs. During these syntheses, we used Ta and Nb tubes as reaction containers, which proved to be less inert than expected. Crystals of $Ta_{4-x}Mo_xGa_5$ and $Nb_{4-x}Mo_xGa_5$ ($x \approx 0.1$) were obtained as side products, which appeared to be related to the $Ta_4Ga_5$ and $Nb_4Ga_5$ phases reported in the Ta−Ga and Nb−Ga phase diagrams,[15,16] but whose crystal structures were hitherto unknown.[14,15] In subsequent syntheses in these binary systems, we were able to confirm this relationship by obtaining $Ta_4Ga_5$ and $Nb_4Ga_5$ as major phases and solving their structures using single-crystal X-ray diffraction.

As we will see, their structures correspond to a new binary structure type, $Ta_4Ga_5$, which can be easily visualized in terms of a hierarchical relationship[9,16−18] to the simple Heusler structure type, as exemplified by $MnAlCu_2$ (Figure 1).[19,20] In the $MnAlCu_2$ structure, the Cu atoms form a primitive cubic network (gray), with the Mn and Al atoms filling the cubic holes in an alternating fashion (blue and yellow). In the $Ta_4Ga_5$ type, a similar pattern is encountered, with clusters occurring in place of individual atoms: the primitive cubic framework is built from Ta body-centered-cubic (bcc) units, whose square faces are capped by Ga, while the cubic holes are occupied by pseudoicosahedral clusters and pairs of bcc fragments.

Throughout this structure there is a tendency for the transition metal (T) and Ga atoms to coalesce into

Special Issue: To Honor the Memory of Prof. John D. Corbett

Received: August 13, 2014
Published: October 3, 2014

   dx.doi.org/10.1021/ic501966v | Inorg. Chem. 2015, 54, 821−831

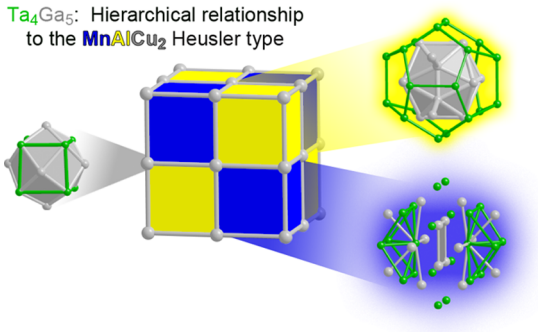


**Figure 1.** Structural features of the new binary structure type adopted by $Ta_4Ga_5$ and $Nb_4Ga_5$, illustrated by its hierarchical relationship to the $MnAlCu_2$ (Heusler) type.

homoatomic clusters, such as T bcc units, Ga tetrahedra, and Ga icosahedra. This apparent dominance of homoatomic clusters appears to be at odds with the usual expectation that heteroatomic interactions provide the impetus for binary phase formation. Using DFT-calibrated Hückel calculations and the reversed approximation molecular orbital (raMO) analysis,[21] we will trace these geometrical features to the dominance of T−T interactions in forming a pseudogap at the Fermi energy, and the role of Ga atoms in preferentially stabilizing T−T bonding states over T−T antibonding ones. The resulting bonding picture offers a view into how the balance between homoatomic and heteroatomic interactions can influence the shapes of clusters in intermetallic phases.

## 2. EXPERIMENTAL SECTION

**2.1. Syntheses.** Our first crystal exhibiting the $Ta_4Ga_5$ type was obtained upon heating Ga (Strem chemicals, 99.99%) and Mo (Strem chemicals, 99.95%) in a 5.0 mm diameter Ta tube (American Elements, 99.9%). The elements were weighed in a molar ratio of Ga:Mo = 5:1 in an Ar-filled glovebox and placed in a Ta tube. The Ta tube was welded shut using an arc-melting furnace and sealed in an evacuated fused-silica ampule. The sample tube was annealed at 800 °C for 120 h. Attempts to prepare phase-pure $Ta_4Ga_5$ were then made. In the most successful of these syntheses, Ta foil (Sigma-Aldrich, >99.9%) and Ga (Strem chemicals, 99.99%) were used as starting materials (following the procedure for transition metal gallide synthesis of Girgis[22]), with a small amount of $I_2$ added to promote vapor-phase diffusion and crystal growth. The elements were weighed in the stoichiometric molar ratio Ta:Ga:I = 4:5:0.0001 and placed in a fused-silica tube. After being evacuated and sealed, the tube was annealed at 850 °C for 700 h.

$Nb_4Ga_5$ was similarly first identified as a side reaction of Ga with a Nb reaction container during synthetic explorations using Ga as a flux. Phase-pure $Nb_4Ga_5$ was then synthesized by loading stoichiometric amounts of Nb powder (Strem Chemicals, 99.8%) and Ga shot (Strem Chemicals, 99.99%) into an alumina crucible in an Ar-filled glovebox. The alumina crucibles were then placed in fused-silica tubes, which were transferred to a vacuum line (with care taken to avoid exposure to atmospheric $O_2$), and sealed under vacuum (~100 mTorr). The tubes were next set vertically in a muffle furnace, heated to 1100 °C in 5.5 h, held at this temperature for 198 h, and cooled to room temperature over 11 h.

**2.2. Single-Crystal X-ray Diffraction Analysis.** Single-crystal X-ray diffraction data for the original $Ta_4Ga_5$-type crystal ($Ta_{3.86}Mo_{0.14}Ga_5$) and crystals from the binary $Ta_4Ga_5$ and $Nb_4Ga_5$ syntheses were collected at room temperature on a Bruker Quazar SMART APEX2 diffractometer with a Mo K$\alpha$ microfocus source ($\lambda$ = 0.71073 Å). Unit cell determination and peak integration were performed using the *SAINT*, version 8.34A, software package supplied

**Table 1. Crystal Data for $Ta_{3.86}Mo_{0.14}Ga_5$, $Ta_4Ga_5$, and $Nb_4Ga_5$[a]**

| | | | |
|---|---|---|---|
| chemical formula | $Ta_{3.86}Mo_{0.14}Ga_5$[b] | $Ta_4Ga_5$ | $Nb_4Ga_5$ |
| EDS/WDS composition | $Ta_{3.92(12)}Mo_{0.12(2)}Ga_{4.97(13)}$[c] | $Ta_{4.04(12)}Ga_{4.96(12)}$[d] | $Nb_{4.02(7)}Ga_{4.98(7)}$[d] |
| space group | $P4_2/mnm$ (No. 136) | $P4_2/mnm$ (No. 136) | $P4_2/mnm$ (No. 136) |
| $a$ [Å] | 11.78000(10) | 11.78880(10) | 11.8279(11) |
| $c$ [Å] | 16.9547(2) | 16.9818(3) | 17.0691(15) |
| cell volume | 2352.78(4) | 2360.06(5) | 2388.0(4) |
| $Z$ | 16 | 16 | 16 |
| Pearson symbol | $tP144$[e] | $tP144$[e] | $tP144$ |
| cryst dimens [mm$^3$] | 0.05 × 0.03 × 0.01 | 0.02 × 0.01 × 0.005 | 0.02 × 0.02 × 0.01 |
| crystal color, habit | metallic black, plate | metallic black, irregular | metallic gray, irregular |
| data collection temp | RT | RT | RT |
| radiation source, $\lambda$ [Å] | Mo K$\alpha$, 0.7107 | Mo K$\alpha$, 0.7107 | Mo K$\alpha$, 0.7107 |
| abs coeff [mm$^{-1}$] | 93.351 | 96.257 | 29.428 |
| abs corrn | multiscan | multiscan | multiscan |
| $\theta_{min}$, $\theta_{max}$ | 2.11, 33.39 | 2.1, 33.45 | 2.09, 32.6 |
| no. of reflns | 69406 | 60353 | 46270 |
| unique reflns [$I > 3\sigma(I)$, all] | 2349, 2462 | 2046, 2469 | 1843, 2374 |
| refinement method | $F^2$ | $F^2$ | $F^2$ |
| $R_{int}$ [$I > 3\sigma(I)$, all] | 4.55, 4.56 | 4.22, 4.48 | 5.30, 5.94 |
| no. of param | 106 | 106 | 99 |
| $R$, $R_w$ [$I > 3\sigma(I)$] | 0.0200, 0.0656 | 0.0156, 0.0341 | 0.0172, 0.0386 |
| $R$, $R_w$ (all) | 0.0223, 0.0787 | 0.0244, 0.0377 | 0.0289, 0.0423 |
| $S$ [$I > 3\sigma(I)$], $S$ (all) | 2.29, 2.68 | 1.58, 1.59 | 1.07, 1.03 |
| $\Delta\rho_{max}$, $\Delta\rho_{min}$ (e Å$^{-3}$) | 2.44, −3.12 | 2.30, −2.36 | 1.71, −1.41 |

[a]Crystallographic information files containing further details for $Ta_{3.86}Mo_{0.14}Ga_5$, $Ta_4Ga_5$, and $Nb_4Ga_5$ can be obtained from the Fachinformationszentrum Karlsruhe (e-mail: crysdata@fiz-karlsruhe.de), upon quoting the depository numbers 428175, 428173, and 428174, respectively. [b]Preliminary structure model. See the text for details. [c]WDS composition. [d]EDS composition. [e]The Pearson symbol refers to an idealized disorder-free version of the structure, in which the <2% occupancies of the Ta8 and Ta9 sites are rounded to zero.


dx.doi.org/10.1021/ic501966v | *Inorg. Chem.* 2015, 54, 821−831

Table 2. $Ta_4Ga_5$ Atomic Coordinates and Displacement Parameters

| site | Wyckoff position | $x$ | $y$ | $z$ | $U_{eff}$ | occupancy |
|---|---|---|---|---|---|---|
| Ta1 | 16d | 0.495017(17) | 0.207012(17) | 0.146334(13) | 0.00404(6) | 1.0 |
| Ta2 | 8d | 0.753450(18) | 0.246550(18) | 0.101243(17) | 0.00383(6) | 1.0 |
| Ta3 | 8d | 0.34746(2) | 0.14424(2) | 0 | 0.00372(7) | 1.0 |
| Ta4 | 4d | 1/2 | 0 | 1/4 | 0.00286(8) | 1.0 |
| Ta5 | 4d | 0.38351(2) | 0.38351(2) | 0 | 0.00529(8) | 1.0 |
| Ta6 | 8d | 0.390805(17) | 0.609195(17) | 0.258047(17) | 0.00460(6) | 1.0 |
| Ta7 | 16d | 0.298033(17) | 0.011915(17) | 0.148626(13) | 0.00375(6) | 1.0 |
| Ta8[a] | 8d | 0.3900(11) | 0.3900(11) | 0.2392(11) | 0.010(4) | 0.0176(13)[b] |
| Ta9[a] | 4d | 0.1171(15) | 0.1171(15) | 0 | 0.010(4) | 0.0176(15)[b] |
| Ga1 | 8d | 1/2 | 0 | 0.07756(5) | 0.0050(2) | 1.0 |
| Ga2 | 8d | 0.24883(7) | 0.93523(7) | 0 | 0.0079(2) | 1.0 |
| Ga3 | 8d | 0.57159(7) | 0.21779(7) | 0 | 0.0066(2) | 1.0 |
| Ga4 | 8d | 0.11666(5) | 0.11666(5) | 0.07435(5) | 0.00631(17) | 0.9824(15) |
| Ga5 | 16d | 0.17015(5) | 0.33378(5) | 0.25994(3) | 0.00451(14) | 1.0 |
| Ga6 | 8d | 0.26136(5) | 0.26136(5) | 0.12618(5) | 0.00490(16) | 1.0 |
| Ga7 | 8d | 0.59051(5) | 0.40949(5) | 0.08795(5) | 0.00615(17) | 1.0 |
| Ga8 | 8d | 0.40429(5) | 0.40429(5) | 0.34108(5) | 0.00810(19) | 0.9824(13)[b] |
| Ga9 | 8d | 0.40930(5) | 0.40930(5) | 0.18043(5) | 0.00632(18) | 0.9824(13)[b] |

[a]Atoms refined isotropically. [b]These partial occupancies are interpreted in terms of cluster disorder; see ref 34.

by the manufacturer. Scaling and absorption correction were executed with *SADABS*. The structures were solved with the charge-flipping algorithm[23,24] using the program *SUPERFLIP*[25] and refined on $F^2$ using the program *JANA2006*.[26] The Fourier electron densities and surfaces separating the $Ta_4Ga_5$ structure into Ta- and Ga-rich domains were visualized with the program *VESTA3*.[27] Further details regarding the refinements and structure models are given in Tables 1 and 2 and in the Supporting Information.

**2.3. Powder X-ray Diffraction Analysis.** The phase composition of the samples was analyzed using powder X-ray diffraction. Material from each sample was ground to a fine powder and placed on a zero-background plate. Data were measured on a Bruker D8 Advance powder diffractometer with Cu K$\alpha$ radiation ($\lambda$ = 1.5418 Å) at ambient temperature. Diffraction intensities were measured using a LYNXEYE detector with a 2$\theta$ range of at least 20−80° (increment = 0.01°), with exposure times of 0.7 s or longer. The diffraction patterns were analyzed using the programs *Match!*, version 2.0.9, and *JANA2006*.

**2.4. Energy-Dispersive X-ray Spectroscopy (EDS).** Semi-quantitative determinations of the elemental compositions of the $Ta_4Ga_5$ and $Nb_4Ga_5$ phases were performed using EDS. The crushed samples were suspended in epoxy and then polished by hand with a diamond-lapping film down to 0.5 $\mu$m grit. A 20-nm-thick layer of C was evaporated onto the sample to avoid charging due to the nonconductive epoxy. The polished and coated samples were then examined with a Hitachi S-3100N scanning electron microscope equipped with an EDS probe (voltage: 15 keV). The measurement of 23 random points on both $Ta_4Ga_5$ and $Nb_4Ga_5$ revealed only one phase to be present, consistent with powder X-ray diffraction results. The averaged composition, excluding C from the conductive coating, was determined to be $Ta_{4.04(12)}Ga_{4.96(12)}$ from the Ta M and Ga L shell emission lines for $Ta_4Ga_5$ and $Nb_{4.03(6)}Ga_{4.97(6)}$ from the Nb L and Ga K$\alpha$ shell emission lines for $Nb_4Ga_5$. No other elements were observed.

**2.5. Electron Probe Microanalysis (EPMA).** Determination of the elemental composition of the $(Ta/Mo)_4Ga_5$ phase was performed using EPMA. To prepare the sample for EPMA measurements, a small amount of the sample material was suspended in epoxy at one end of a short segment of Al tubing. The tube was then ground down to produce a smooth flat surface and polished to reduce the number of surface scratches using a polycrystalline diamond suspension spread on a polishing wheel. As a final step, the sample tube and standards were coated with 250 nm of graphitic carbon and inspected with a Cameca SX-51 electron microprobe using a voltage of 15 kV and a 30 nA Faraday cup current with a fully focused beam (estimated beam diameter of 500 nm). Ta metal (Sigma-Aldrich, >99.9%), Mo metal (provided by the EPMA standard supplier, Tousimis Research Co., 99.97%), and Ga metal (Strem Chemicals, 99.99%) were used as standards because the sums of the percentages were close to 100%. The data were processed with the *Probe for EPMA* software, using the Pouchou and Pichoir model for the matrix correction.[28]

Measurements were taken on a number of random points on the sample materials. A total of 11 of these showed compositions close to the expected $(Ta/Mo)_4Ga_5$ composition and gave the average composition of $Ta_{3.92(12)}Mo_{0.12(1)}Ga_{4.97(13)}$, which corresponds well to the $Ta_{3.86}Mo_{0.14}Ga_5$ composition from single-crystal structure refinement. The remainder of the points corresponded to phases with approximant compositions $Ta_3Ga_2Mo_x$ ($0.05 < x < 0.13$) and $TaGaMo_{0.2}$.

**2.6. Electronic Structure Calculations.** First principles DFT calculations utilizing the generalized gradient approximation (GGA) were performed on the $Ta_4Ga_5$-type phases $Ta_4Ga_5$ and $Nb_4Ga_5$ using the Vienna Ab Initio Simulation Package (VASP),[29,30] with ultrasoft pseudopotentials provided with the package.[31] All calculations were carried out in the high-precision mode, corresponding to energy cutoffs of 218.21 and 218.46 eV for $Ta_4Ga_5$ and $Nb_4Ga_5$, respectively, and employed Γ-centered 6 × 6 × 4 $k$-point meshes. Geometrical optimization of the crystal structures was performed by first relaxing the ionic positions and then releasing all structural parameters. Once the ground-state structures were reached, single-point calculations were made to obtain band energies and density of states (DOS) curves.

The output of the GGA-DFT calculations then provided the basis for the parametrization of effective Hückel models using the *eHtuner* program,[32] which utilizes a modified version of *YAeHMOP*[33] for the actual Hückel calculations. *YAeHMOP* was then used to obtain DOS distributions and crystal orbital Hamilton population (COHP) curves for the structures as well as for the calculation of the Hamiltonian matrix for the Γ point of a 2 × 2 × 2 supercell of $Ta_4Ga_5$. The Γ-point Hamiltonian was then imported into *MATLAB*, where raMO analyses were carried out using in-house functions.

## 3. RESULTS AND DISCUSSION

**3.1. Synthesis and Identification of $Ta_4Ga_5$-Type Phases.** Our first crystal exhibiting $Ta_4Ga_5$-type features was found during a synthetic exploration of the Mo−Ga system using welded Ta tubes as reaction containers. One of the crystals we selected from the synthesis products exhibited an X-


dx.doi.org/10.1021/ic501966v | Inorg. Chem. 2015, 54, 821−831

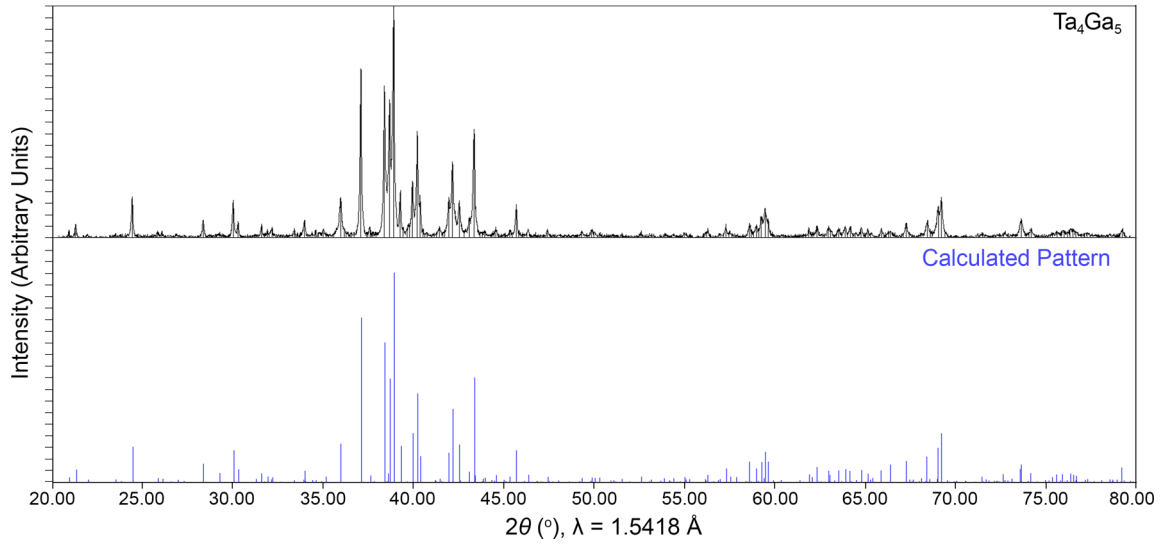


**Figure 2.** Powder X-ray diffraction pattern of $Ta_4Ga_5$. The top panel gives the experimental pattern for a $Ta_4Ga_5$ sample, while the bottom panel shows, for comparison, the intensities calculated from the structure model refined from a single-crystal X-ray diffraction data set.

ray diffraction pattern consistent with a tetragonal 11.78 Å × 11.78 Å × 16.98 Å unit cell. In a search for similar cells in the transition metal gallide phase diagrams, we found that the $Nb_4Ga_5$ phase is listed as adopting a tetragonal 8.4 Å × 8.4 Å × 17.1 Å unit cell (but whose structure remained undetermined),[35] which can be approximately transformed to match our crystal's by multiplying the *a*- and *b*-axis lengths by $\sqrt{2}$. On the basis of this metrical relationship, we suspected that we had obtained $Ta_4Ga_5$ or a Mo-substituted variant. Our crystal structure solution and refinement supported this hypothesis, yielding a refined composition of $Ta_{3.9}Mo_{0.1}Ga_5$.

After inspection of the Ta−Ga phase diagram in more detail, this synthetic result was somewhat surprising to us. $Ta_4Ga_5$ appears here as a low-temperature phase that undergoes peritectoid decomposition into $TaGa_3$ and $Ta_3Ga_2$. At no point does it occur in equilibrium with a melt, making the growth of high-quality crystals such as the one obtained in our synthesis difficult. Nevertheless, through experimentation with a variety of synthetic approaches (see the Experimental Section), we were able to synthesize samples in the Ta−Ga and Nb−Ga binary systems whose powder patterns' major peaks are consistent with binary versions of the $Ta_{3.9}Mo_{0.1}Ga_5$ phase obtained earlier (Figure 2). Analysis of crystals selected from these samples revealed that $Ta_4Ga_5$, $Nb_4Ga_5$, and $Ta_{3.9}Mo_{0.1}Ga_5$ are closely related. $Ta_4Ga_5$ and $Nb_4Ga_5$ are isostructural and appear to represent a new binary structure type.

The strongest reflections for the $Ta_{3.9}Mo_{0.1}Ga_5$ crystal are also consistent with this structure type. A structural refinement with this model leads to reasonable agreement between the calculated and experimental single-crystal X-ray diffraction intensities and yields a Mo content (through partial substitution on the Ta6 and Ta7 sites) that matches that obtained through microprobe measurements. However, close inspection of the diffraction pattern reveals weak superstructure reflections that violate the systematic absence conditions stemming from the *n* glide of the $P4_2/mnm$ space group. We plan to characterize of this superstructure in conjunction with more systematic studies of Mo substitution. For now, we include the results of our refinement using a preliminary $P4_2/mnm$ model in Table 1 and the Supporting Information.

**3.2. Structural Description of the $Ta_4Ga_5$ Type.** The basis of all three phases described in this Article is a new structure type. We will refer to this as the $Ta_4Ga_5$ type and focus our discussion on this prototype phase. The $Ta_4Ga_5$ structure is relatively complex, with seven and nine symmetry-distinct Ta and Ga sites, respectively. For $Ta_4Ga_5$ and $Ta_{3.9}Mo_{0.1}Ga_5$, additional sites with very low occupancy (e.g., ca. 2% for Ta8 and Ta9 in Table 2) were uncovered by inspection of the Fourier difference maps. Here, we will restrict ourselves to the sites with full or nearly full occupancy, which encode for a total of 144 atoms per unit cell, while our interpretation of the Ta8 and Ta0 sites in terms of cluster disorder can be found in ref 34.

The process of understanding this structure is made considerably simpler by the observation that it is based on an approximately primitive cubic substructure (Figure 3). To see this, we begin by noting that the Ta4 site, which occurs at the high-symmetry 4d positions, forms the center of a small

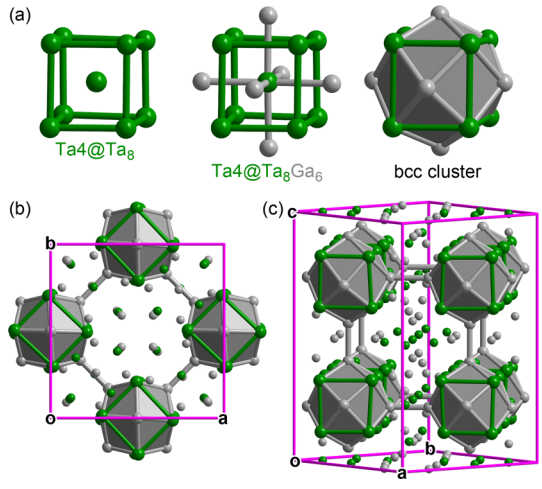


**Figure 3.** The primitive cubic substructure of the $Ta_4Ga_5$ structure type. (a) $Ta4@Ta_8Ga_6$ bcc fragment that occurs at the nodes of the primitive cubic framework. (b and c) Two views of the cubic substructure shown in the context of the full unit cell.


dx.doi.org/10.1021/ic501966v | *Inorg. Chem.* 2015, 54, 821−831

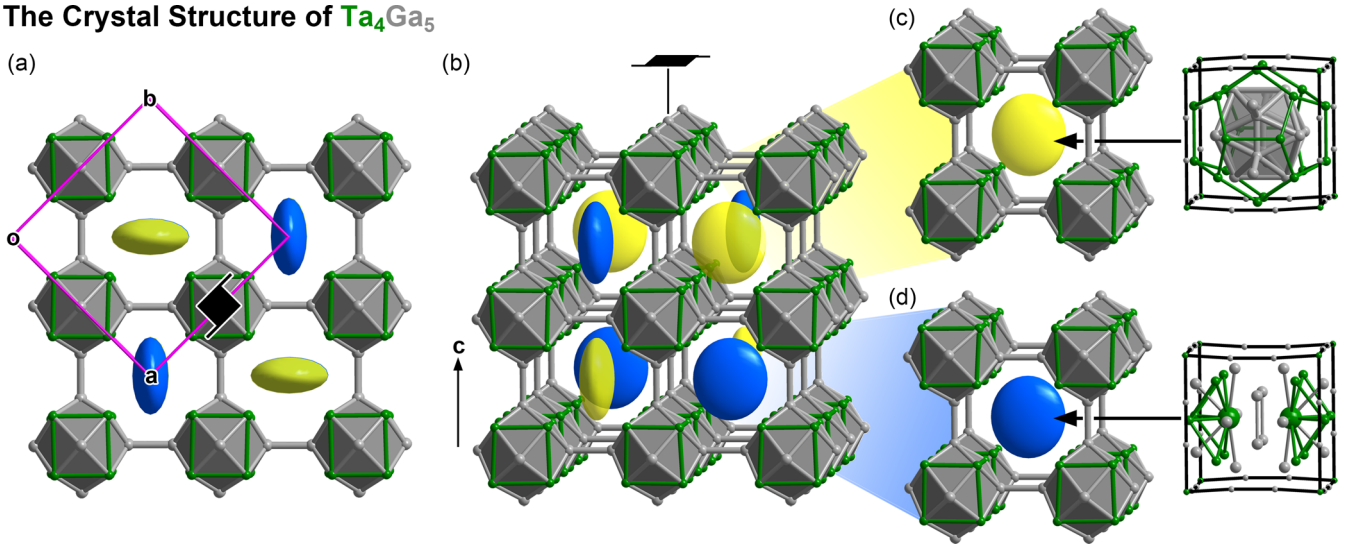


**Figure 4.** The full crystal structure of $Ta_4Ga_5$, viewed in terms of the filling of a primitive cubic host substructure. The $Ta_4Ga_5$ structure is first viewed (a) along and (b) approximately perpendicular to the *c* axis, with yellow and blue ellipsoids indicating the type and orientation of the occupants of each cubic void space. (c) Yellow ellipsoids signify pseudoicosahedral units centered by flattened $Ga_{12}$ icosahedra that are enclosed in Ta pentagonal dodecahedra. (d) Blue ellipsoids stand for dimers of $Ta_7Ga_6$ bcc fragments separated by Ga squares. See Figure 1 for parallels to the $MnAlCu_2$ (Heusler) structure type.

fragment of the bcc structure (Figure 3a). The Ta4 site is surrounded by a cube of Ta atoms (Ta4@$Ta_8$), whose faces are capped by Ga to create a rhombic dodecahedron, the coordination polyhedron of the bcc structure. These Ta4@$Ta_8Ga_6$ clusters pack in a primitive cubic fashion (Figures 3b,c) and are linked through Ga−Ga contacts.

The nearly cubic symmetry of this framework is broken by the contents of its void spaces, which are represented in Figure 4a,b by ellipsoidal shapes chosen to capture the symmetry relationships among the occupants of the holes. Half of the spaces are filled with distorted icosahedral motifs (yellow ellipsoids in Figure 4a,c): flattened $Ga_{12}$ icosahedra center these void spaces and are enclosed by $Ta_{20}$ pentagonal dodecahedra derived from both additional guest atoms and atoms from the $Ta_8$ cubes of the host framework.

These icosahedra-stuffed voids alternate with another set of spaces in which the contents form a less recognizable pattern (blue ellipsoids in Figure 4a,d). The centers of the cubic holes are occupied by a pair of Ta atoms at a large distance of nearly 4.0 Å, bisected by a square of Ga atoms. The remainder of the space around each Ta atom in the pair resembles a partially successful attempt to create the $Ta_8Ga_6$ coordination environment of the Ta4 sites.

This arrangement of clusters mirrors the atomic arrangements in a much simpler intermetallic structure type: the $MnAlCu_2$ Heusler type (Figure 1). In $MnAlCu_2$, the Cu atoms are arrayed in a primitive cubic network, whose holes are occupied by Mn and Al atoms, similar to the CsCl type. However, rather than randomly occupying the cubic holes, the Mn and Al atoms are placed in an alternating fashion. The basic features of the $Ta_4Ga_5$ type are obtained by replacing the Cu atoms of $MnAlCu_2$ with Ta4@$Ta_8Ga_6$ bcc clusters, the Al atoms with the pseudoicosahedral units (Figure 4c), and the Mn atoms with the bcc fragment dimers (Figure 4d).[34]

**3.3. Visualizing Elemental Domains within the $Ta_4Ga_5$ Structure.** In each of these structural features, a surprising theme is encountered: the prominence of homoatomic interactions. For instance, the bcc fragments at the vertices of the cubic substructure are centered by clusters of Ta atoms, while the pseudoicosahedral units are nucleated by $Ga_{12}$ clusters. This trend is also evident in the coordination environments of the individual Ta and Ga sites of the structure. In Figure 5, we show the surroundings of the seven symmetry-distinct Ta sites in the structure, with Ta−Ta and Ga−Ga contacts within the coordination shells highlighted. For all but the Ta4 site, the Ta and Ga neighbors to the central atom appear largely aligned toward opposite poles, creating homoatomic domains that seem to clasp each other around the central atom.

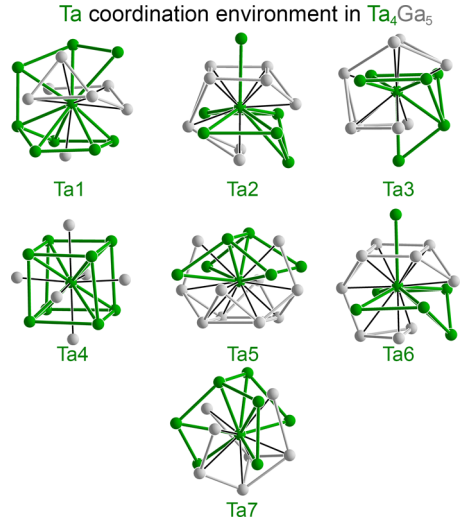


**Figure 5.** Coordination environments for the seven symmetry-distinct Ta sites in $Ta_4Ga_5$. Ta−Ta and Ga−Ga contacts within the polyhedra are shown to emphasize the prominence of homoatomic interactions.

The segregation of Ta−Ta and Ga−Ga interactions is more pronounced in the coordination environments of the Ga atoms (Figure 6). In these polyhedra, the Ta atoms adopt two basic types of arrangements: pentagonal rings that encircle the


dx.doi.org/10.1021/ic501966v | Inorg. Chem. 2015, 54, 821−831

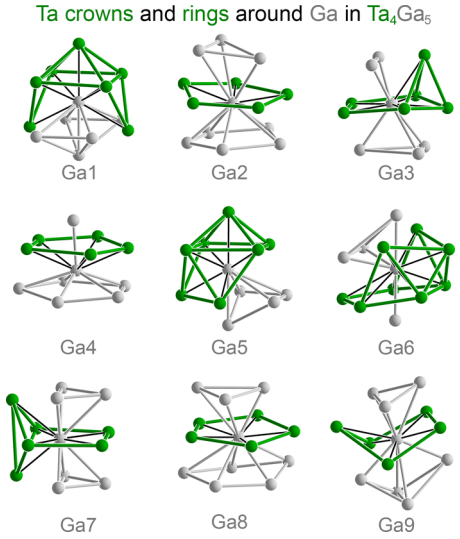


**Figure 6.** Coordination environments of the Ga sites in $Ta_4Ga_5$, which exhibit clustering of the Ta neighbors into rings and partial cages.

central Ga atom (Ga2−Ga4 and Ga6−Ga9) or crowns based on Ta square pyramids with some basal edges capped (Ga1 and Ga5). The Ga neighbors then fill in the remaining spaces.

In both the Ta and Ga coordination environments, a spatial division of the atoms into Ta- and Ga-rich domains is observed. How does this apply to the crystal structure as a whole? One way to visualize the presence of such domains in the structure is to attempt to draw interfaces between the Ta and Ga regions. In Figure 7, we illustrate one such surface derived from

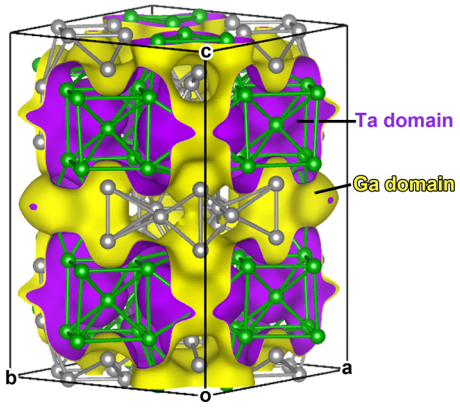


**Figure 7.** Geometrically constructed surface separating the $Ta_4Ga_5$ structure into Ta and Ga domains. The atoms on the yellow side of the surface are exclusively Ga, while those on the purple side are all Ta. See the text for details.

geometrical considerations.[36] This surface divides the structure into two three-dimensionally continuous domains, showing that the $Ta_4Ga_5$ phase can be interpreted in terms of two interpenetrating regions, one Ta-rich and the other Ga-rich. In fact, all of the Ga atoms in the structure lie on the yellow side, while all of the Ta atoms are positioned on the purple side.

This ability to draw surfaces between the sublattices of two different elements in a binary structure in itself is not unique, as such could easily be done with, say, the double-diamond framework of the NaTl Zintl phase.[37] What is surprising about this surface, however, is the thickness of the domains in many places. For example, at the center of the view in Figure 7 is a clustering of Ga tetrahedra on the yellow side of the surface, which is surrounded by Ta bcc fragments on the purple side.

The surface of Figure 7 in some ways recalls the use of minimal surfaces or periodic nodal surfaces in interpreting crystal structures.[38−41] A comparison between the current surface and minimal surfaces, in particular, is informative about the nature of the segregation between the Ta and Ga atoms in $Ta_4Ga_5$. One reason that minimal surfaces are so useful in discussing biphasic phenomena is that they represent the surface-area minimization expected for domains of incompatible bonding types, such as polar and nonpolar. However, in the case of Figure 7, the surface exhibits bulges of one domain into another; here, the interfacial area is far from being minimized. Based on this observation, we may conclude that Ta−Ga interactions are not simply minimized but represent an important contributor to the stability of the structure.

For those of us who expect heteroatomic interactions to be the driving force for binary phase formation, this conclusion about the importance of Ta−Ga bonding is comforting. At the same time, however, it makes the division of the structure into clear Ta and Ga domains more mysterious. In the next section, we will discover that this simultaneous attraction and repulsion between Ta and Ga has origins in multicenter bonding and the nodal properties of the Ga atoms' valence orbitals.

**3.4. Electronic Structure of $Ta_4Ga_5$.** In order to understand the origins of the unique host−guest features and homoatomic clustering of the $Ta_4Ga_5$ type, we carried out GGA-DFT calculations on geometrically optimized structures of $Ta_4Ga_5$ and $Nb_4Ga_5$. As in our structural description above, we will focus on the compound $Ta_4Ga_5$ as a representative of this structure type. For our calculations on this compound, we prepared a slightly idealized structure model, in which the partial occupancies of ca. 98% and 2% for a handful of sites are rounded to 1 or 0, respectively.

The electronic DOS curve obtained for $Ta_4Ga_5$ (the result for $Nb_4Ga_5$ was very similar; see the Supporting Information) is shown in Figure 8a. As with other T−E intermetallics, the DOS

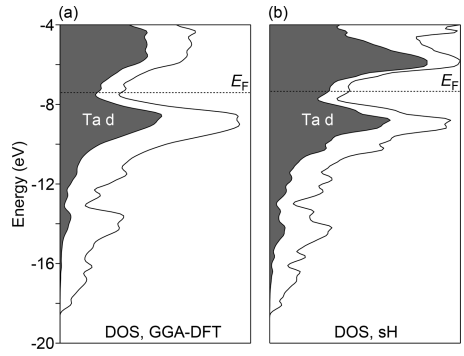


**Figure 8.** Electronic DOS distributions calculated for $Ta_4Ga_5$ using (a) GGA-DFT and (b) a DFT-calibrated simple Hückel (sH) model. Shaded regions correspond to the contributions from Ta d character. The curves have been treated with Gaussian broadening to make their general features more apparent.

distribution can be seen as approximately a superposition of a parabolic nearly free-electron DOS that stretches to low energies and a more narrow distribution of T d orbital-based states at an intermediate energy. The Fermi energy ($E_F$) of the phase lies in a deep well in the DOS that approximately bisects the Ta d block of states. This coincidence of a pseudogap with


dx.doi.org/10.1021/ic501966v | Inorg. Chem. 2015, 54, 821−831

the transition between filled and empty states strongly indicates that the structure is stabilized by a favorable band filling.

To gain deeper insight into the origin of this pseudogap, we used the band energies and DOS curves from our DFT calculations as the basis for parametrization of a simple Hückel model for $Ta_4Ga_5$. Using our program *eHtuner*,[32] we were able to obtain a simple Hückel model reproducing the DFT band energies with a root-mean-squared deviation of 0.085 eV (for bands up to 1 eV above the $E_F$).

The DOS distribution calculated using this model is shown alongside the DFT result in Figure 8b. While some differences can be noted between the two distributions (particularly above the $E_F$ values), there are important similarities: the Hückel model reproduces the shape of the DOS distribution below the $E_F$, as well as the energy ranges of its various broad features. Also, the $E_F$ again lies in a deep opening in the DOS distribution, separating two dense mounds of states that are rich in Ta d character. Together these correspondences suggest that the favorability of the phase's electron count should be understandable from the point of view of orbital interactions using this effective Hückel model for the DFT results.

Now that we have established this Hückel model, let us use it to probe deeper into the origins of the DOS pseudogap at the $E_F$. First, the relative importance of the various interatomic interactions present in the compound can be evaluated through calculation of crystal orbital Hamilton population (COHP) curves,[42] in which the DOS distribution is weighted by its component states' energetic contributions to a given interaction. In Figure 9, we plot the COHP curves for the Ta−Ta

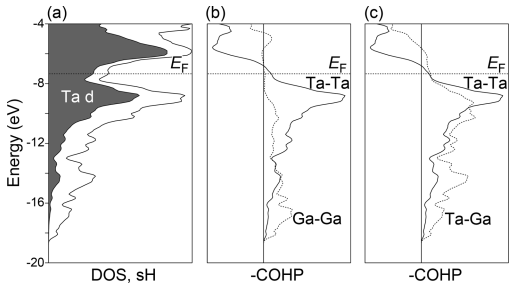


**Figure 9.** Crystal orbital Hamilton population (COHP) curves for the homoatomic and heteroatomic interactions in $Ta_4Ga_5$. (a) The simple Hückel DOS distribution shown for comparison with the COHP curves. (b) COHP curves for the Ta−Ta (solid) and Ga−Ga interactions (dotted). (c) The Ta−Ga COHP curve (dotted) plotted along with the Ta−Ta curve for reference.

(Figure 9b,c), Ga−Ga (Figure 9b), and Ta−Ga (Figure 9c) interactions in the structure. For all three curves, the COHP function is negative at low energies, corresponding to favorable bonding interactions, and remains negative for all of the occupied states. The transitions to antibonding character occur at various points above the $E_F$. The first to switch from bonding to antibonding is the Ta−Ta curve, whose transition occurs slightly above the $E_F$. The Ta−Ga curve displays antibonding character at higher energies (ca. −6 eV), while the Ga−Ga curve wobbles about the $x = 0$ axis above the $E_F$ before settling on antibonding character at around −4 eV.

From these COHP curves, it appears that all three interaction types contribute significant bonding to the phase. In terms of the pseudogap, however, the Ta−Ta interactions appear to be especially important: the optimization of Ta−Ta bonding coincides closely with the top of the pseudogap region, suggesting that the gap represents a separation of Ta−Ta bonding and antibonding states. The presence of such Ta−Ta bonding interactions is consistent with the structures' Ta−Ta interatomic distances (2.85−3.64 Å in Figure 5, the shortest of which are below the sum of the metallic radii, 2.92 Å).

This transition between Ta−Ta bonding and antibonding character occurs at an electron concentration that is about 0.5 electrons/Ta atom higher than the 8.75 electrons/Ta atom calculated from the formula unit. This small deficiency could explain the ability of the structure to accommodate some substitution with Mo on the Ta sites, as is seen in $Ta_{3.9}Mo_{0.1}Ga_5$, since each Mo atom incorporated increases the number of valence electrons by one.

Based on the position of the DOS pseudogap, it appears that about nine electrons per Ta atom is a particularly favorable electron count for this phase. What underlies this special electron count? Through bonding analyses on a number of intermetallics formed between transition metals (T) and metalloid elements, we have found that similar pseudogaps could be explained in terms of the 18-electron rule of molecular transition metal complexes. From this point of view, the special stability is obtained when nine electron pairs are associated with a transition metal center, one for each of its nine s, p, and d valence orbitals. For compounds containing T atoms that are isolated from each other, such as $NiSi_2$,[43] $Fe_8Al_{17.4}Si_{7.6}$,[43] and $CrGa_4$,[21] this rule translates into the presence of DOS pseudogaps at 18 electrons/transition metal atom. When T−T contacts are present, as in $Co_3Al_4Si_2$,[44] the sharing of electron pairs between the transition metal atoms allows for 18-electron configurations to be achieved with a smaller number of valence electrons per T: $18 - n$, where $n$ is average number of electron pairs that each T atom shares with other T atoms.

These considerations lead to a hypothesis for the location of the pseudogap in $Ta_4Ga_5$ near 9 electrons/Ta atom: this electron count could correspond to $18 - n$ electrons with $n = 9$. In other words, each of the Ta atoms' valence s, p, and d atomic orbitals is involved in Ta−Ta bonding interactions, such that they are split across the DOS pseudogap into bonding and antibonding interactions.

**3.5. raMO Analysis of $Ta_4Ga_5$.** An approach to testing this idea is given by our recently developed raMO method.[21] In this technique, one begins by proposing a simple, localized molecular orbital (MO) diagram to explain the bonding interactions in a local part of a larger molecule or solid. One then tests this analogy by using the occupied one-electron wave functions of the full system as a basis set for the calculation of matrix elements for the Hamiltonian operator corresponding to the model MO diagram. Diagonalization of the resulting matrices leads to two classes of eigenvectors: (1) those with nonzero eigenvectors, corresponding to the best approximation to the true eigenstates of the operator possible using the occupied one-electron wave functions of the full compound (while maintaining orthogonality between the eigenstates) and (2) eigenvectors with eigenvalues of zero. The latter set of solutions consists of functions that are orthogonal to the model MO diagram and thus represent components of one or more separate bonding systems.". In this way, isolobal analogies are used to dissect the electronic structure of a complex molecule or solid into a series of orthogonal bonding systems.

Our tentative association of the valence electron concentration of about 9 valence electrons/Ta atom with a half-filling of the nine valence atomic orbitals for the Ta atoms suggests a very simple MO diagram as a starting point: isolated Ta atoms,


dx.doi.org/10.1021/ic501966v | *Inorg. Chem.* 2015, 54, 821−831

for which the eigenstates are simply the individual atomic orbitals. If this line of thinking is correct, then raMO analyses using Ta s, p, and d as the target states should lead to eigenvectors centered by each of these orbitals, and each of them should show substantial bonding interactions with neighboring Ta atoms.

A first confirmation of this approach can be found by using the full set of s, p, and d orbitals of all of the Ta atoms as target eigenstates. Upon performing the raMO procedure using this model Hamiltonian, only eigenvectors with nonzero eigenvectors are obtained. All electrons in the structure are then associated in some way with the Ta atoms, i.e., there are no functions (corresponding, say, to Ga−Ga interactions) that are orthogonal to all of the Ta orbitals. We are to some extent justified then in expressing the electron concentration in terms of the electrons per Ta atom.

Let us focus our attention now on what these Ta-based functions look like. In Figure 10, we display the raMO

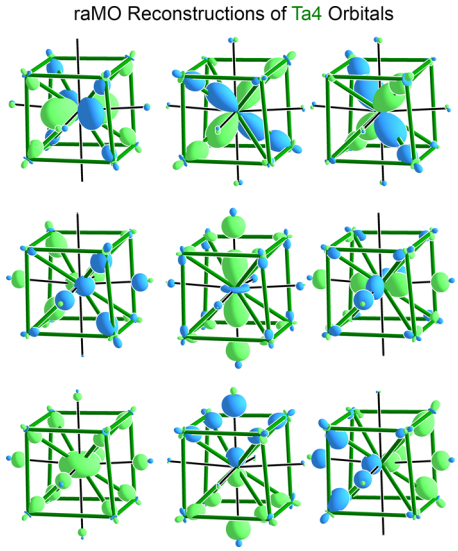


**Figure 10.** raMO reconstructions of the Ta4 site's valence s, p, and d orbitals. See the Supporting Information for a more detailed examination of the degree of localization of these functions.

functions obtained using the s, p, and d orbitals of a Ta atom on the Ta4 site as target eigenstates. An inspection of the orbital character on the central atom of each of their raMO functions indicates that the nine s, p, and d orbitals of the central atom are all represented. However, rather than occurring alone, as would be the case for a nonbonding orbital, all of them exhibit significant in-phase contributions from the surrounding Ga and Ta atoms. This observation is consistent with the results of COHP analysis described above: the Ta atoms are stabilized by substantial Ta−Ta and Ta−Ga bonding.

The ability to use the occupied wave functions to create nine functions localized around the Ta4 site with the symmetry properties of its atomic valence orbitals is highly suggestive of the presence of an 18-electron configuration at this atom. Given the low electron concentration of $Ta_4Ga_5$ (8.75 electrons/Ta), such 18-electron configurations should only be possible with the support of extensive sharing of electrons between Ta atoms. The requisite interactions are readily seen through examination of how the raMO functions spread out from the central Ta4 atom to its neighbors. Its Ta neighbors trace out a slightly distorted cube (green). The central s and p orbitals, as well as $d_{xy}$, $d_{xz}$, and $d_{yz}$, are well oriented for $\sigma$ interactions with these neighboring Ta atoms, and indeed each of their raMO functions exhibits hybrid orbitals on the Ta neighbors (containing s, p, and d character) directed in a bonding fashion toward the central orbital. All seven of these raMO functions represent electron pairs that are involved in significant Ta−Ta bonding. This sharing of electrons between the Ta atoms should be very effective for reducing the necessary electron count for closed-shell electron configurations.

The remaining central orbitals ($d_{z^2}$ and $d_{x^2-y^2}$) have nodal surfaces that pass through the vertices of a cubic coordination environment and are thus not well adapted to $\sigma$ interactions with the Ta neighbors (but do exhibit strong $\sigma$ overlap with lobes on the Ga). Nevertheless, close inspection of the raMO functions reveals contributions from these Ta neighbors: they bear dp hydrids that overlap in a $\pi$ fashion with the central Ta atom's orbital. The presence of these dp hybrids in the raMOs indicates that the appearance of the central $d_{z^2}$ and $d_{x^2-y^2}$ functions in the occupied wave functions of the system is strongly correlated with in-phase combinations of these $\pi$ orbitals. Where $\sigma$ bonding between the Ta atoms is not possible, $\pi$ bonding takes over.

We have now looked in detail at the raMO functions generated for one Ta site, Ta4. On the basis of the very different geometrical arrangements of Ta and Ga neighbors for the other six symmetry-distinct Ta sites, one might expect that raMO analysis would lead to different results. However, the raMO functions generated for the remaining Ta sites are, in fact, remarkably similar, as is illustrated for the Ta2 site in Figure 11 (the corresponding diagrams from the remaining Ta

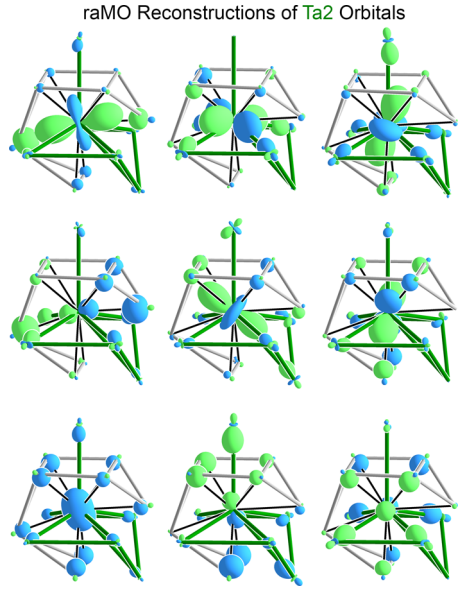


**Figure 11.** raMO functions generated from the occupied crystal orbitals of $Ta_4Ga_5$ using the valence orbitals of an atom on the Ta2 site as target eigenstates.

sites are provided in the Supporting Information). All nine of the central valence orbitals are well-reproduced in the raMOs. Furthermore, each orbital exhibits Ta−Ta bonding interactions of some sort, which is in many cases supported by bridging interactions with Ga atoms. From this point of view, the clustering of the Ta atoms into their own domain in $Ta_4Ga_5$ can


dx.doi.org/10.1021/ic501966v | Inorg. Chem. 2015, 54, 821−831

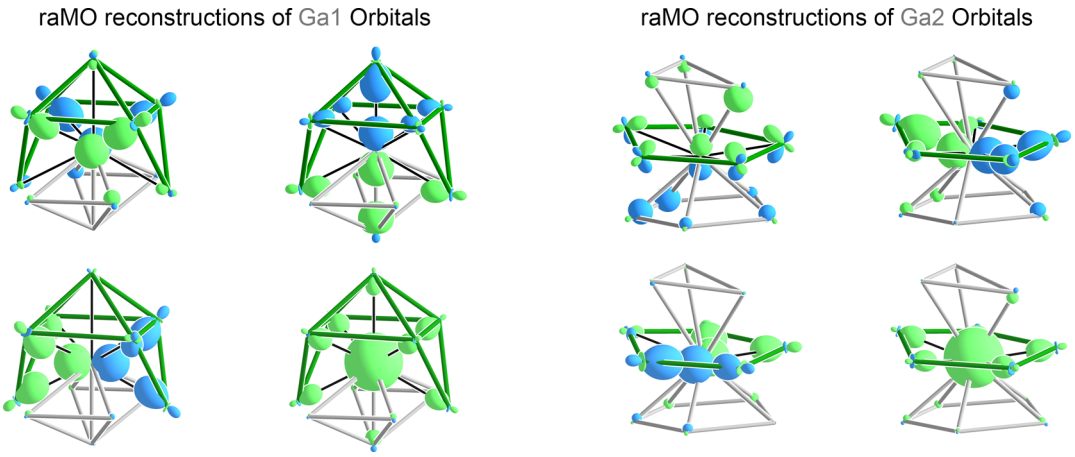


**Figure 12.** raMO functions generated using the valence atomic orbitals of the Ga1 (left) and Ga2 (right) sites in $Ta_4Ga_5$ as target eigenstates. See the Supporting Information for corresponding analyses of the remaining symmetry-distinct Ga sites.

be seen as supporting the extensive Ta−Ta $\sigma$ and $\pi$ interactions needed for the DOS pseudogap at the $E_F$.

A raMO analysis of the Ga sites reveals how their placement in the structure helps widen the DOS pseudogap. In Figure 12, we present raMO functions that result from the use of Ga valence orbitals as target eigenstates, using the Ga1 and Ga2 sites as representative examples (the complete set is provided in the Supporting Information). As we saw for the Ta sites earlier, each of the Ga valence orbitals can be seen at the center of a raMO function. All of the functions exhibit bonding interactions with their Ta neighbors, which are mostly of $\sigma$ character. The prominence of Ta−Ga overlap in these raMOs is consistent with the strong Ta−Ga interactions appearing in our COHP curves. The close matching of the nodal properties of the central Ga atomic orbitals and their surrounding Ta lobes also helps us understand why Ta-centered raMOs are sufficient to reconstruct the full electronic structure of the compound.

This match in the nodal properties also has implications for Ta−Ta bonding in the compound. Note that the small number of nodes passing through the Ga center translates into a small number of nodes switching the phases between adjacent Ta atoms in the Ga atoms' coordination environments (Figure 13).

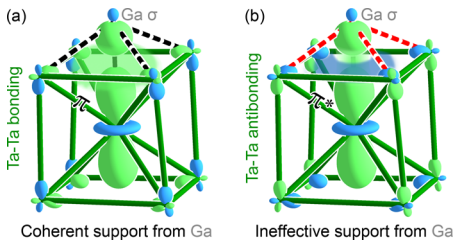


**Figure 13.** Schematic illustration of the preferential support given by bridging Ga atoms to (a) Ta−Ta bonding orbitals over their (b) Ta−Ta antibonding counterparts.

In this way, the clustering of Ta atoms within these polyhedra naturally leads to Ta−Ta bonding because the Ta−Ta antibonding functions for a tightly packed ring or cap of Ta atoms would have too many nodes to be effectively stabilized by the Ga s or p orbitals.

The placement of the Ga atoms at the outskirts of the Ta clusters then means that Ta−Ga bonding takes on a multicenter character that correlates with Ta−Ta bonding. A natural result of this is the nearly simultaneous optimization of the Ta−Ta and Ta−Ga interactions in the COHP curves (Figure 9).

This multicenter bonding character also plays an important role in the formation of the pseudogap at the $E_F$. Because the pseudogap coincides with the Ta−Ta bonding to antibonding transition in the COHP, the ability of the Ga atom to preferentially stabilize the Ta−Ta bonding states should deepen the gap. In fact, a Hückel calculation in which the Ga atoms are removed from $Ta_4Ga_5$ leads to essentially a complete closure of the pseudogap. In this way, the bridging of the Ta−Ta interactions by Ga appears to be essential to the stability of the phase.

In this bonding picture, Ta−Ta and Ta−Ga interactions appear as tightly intertwined, but Ga−Ga interactions have not been assigned a part yet. An examination of the Ga-centered raMOs in Figure 12 reveals that the Ga neighbors join the Ta atoms in decorating the central orbital with bonding lobes. In most cases, however, their contributions are smaller than those of the Ta atoms. They also generally share the lobe of the central atom with Ta neighbors. From these observations, we conclude that the Ga−Ga interactions largely serve to support the wave functions already templated by Ta−Ta and Ta−Ga interactions. However, the tight packing of Ga atoms and the small number of angular nodes in their valence orbitals allow for Ga−Ga bonding overlap to emerge in this situation. Where contributions from the Ga neighbors to the Ga centers of Figure 12 are visible, the interactions are invariably stabilizing.

## 4. CONCLUSIONS

This has been a story of reluctant intermetallic phases that defy the expectation that heteroatomic interactions will dominate the structures of binary compounds. We first described a new binary structure type formed by $Ta_4Ga_5$ (with and without a little Mo substitution) and $Nb_4Ga_5$ from several viewpoints. One approach was through a hierarchical relationship to the Heusler structure type, in which atoms are replaced with clusters. A close variation on this view was recognizing that one set of clusters connect together into a primitive cubic framework that serves as a host matrix for the remaining clusters.

These descriptions are useful in terms of visualizing the structure type, but a deeper connection to the driving forces shaping the structure was made through inspection of the


dx.doi.org/10.1021/ic501966v | Inorg. Chem. 2015, 54, 821−831

individual coordination environments of the atomic sites. Around the majority of the sites, there is a pronounced tendency for the Ga and Ta atoms to collect together into homoatomic clusters. Upon zooming out to see the structure as a whole, we found that the Ta and Ga atoms can be segregated into distinct three-dimensional domains that interpenetrate each other.

Theoretical analysis of the $Ta_4Ga_5$ structure using DFT-calibrated Hückel calculations and raMO analysis revealed how this segregation helps to stabilize the phase. The electronic DOS distributions exhibit a deep well at the $E_F$, a strong indication that a favorable electron configuration has been achieved. This pseudogap can be traced to the clustering of Ta atoms within small angular ranges around the Ga atoms, which allows for correlations between Ta−Ta and Ta−Ga bonding overlap. The multicenter character of the interactions leads to the near-simultaneous optimization of Ta−Ta and Ta−Ga bonding (although for both, weaker tails of bonding extend upward beyond the $E_F$).

The unexpected structural features of this phase have led us to wonder (from the comfortable perspective of hindsight) whether any of these aspects of this structure type could have been anticipated ahead of time. One emerging principle of transition metal−main group (T−E) intermetallics that is especially useful here is the importance of filled 18-electron configurations on the T atom sites. For a growing series of intermetallic compounds, we have been able to connect DOS pseudogaps or band gaps to an association of electron pairs with each of the nine valence orbitals of the T atoms. Where deficiencies are encountered in the electron count relative to 18 electrons/T atom, filled configurations tend to be achieved through the sharing of electron pairs in E-supported T−T bonds.

From this point of view, the clustering of T atoms together could be expected from the valence electron count of $Ta_4Ga_5$. The stoichiometry of the phase gives an average number of electrons per Ta atom of only 8.75, which is less than half of that needed for the Ta atoms to achieve closed shells independently of each other. Extensive sharing of electron pairs between the Ta atoms would thus be needed, which would require substantial clustering of the Ta atoms. Our raMO analysis confirms this bonding picture but falls short of predicting the precise electron count at which the bonding will be optimized. It will be interesting to see whether these correlations between low valence electron count and T/E segregation can be extended to other structures. One example that comes to mind here is the complex rhombohedral structure of MnGa,[45] in which homoatomic clustering similar to that seen in this Article can be perceived in the coordination environments of most of the atomic sites.

A way to screen vast numbers of intermetallic structures for this type of homoatomic clustering would be helpful in testing this hypothesis more broadly. The characteristics of the coordination environments in the $Ta_4Ga_5$ type suggest one approach for such an endeavor. Most of the coordination environments exhibit a polar or quadrupolar distribution of the Ta and Ga atoms. Such distributions could be identified in an automated fashion by assigning a positive or negative number to the two atom types in the coordination shell of each site in a structure and then projecting these numbers onto spherical harmonics. Structures whose atoms have large magnitudes for the low-order functions could then be selected for more detailed structural analysis. We are looking forward to employing this procedure in search of compounds exhibiting chemically frustrated structures.

## ■ ASSOCIATED CONTENT

### Supporting Information

Tables of crystallographic data for the structures presented in this paper, including atomic coordinates and interatomic distances, GGA-DFT optimized coordinates and total energies for $Ta_4Ga_5$ and $Nb_4Ga_5$, additional raMO results for $Ta_4Ga_5$, and electronic DOS curves for $Nb_4Ga_5$. This material is available free of charge via the Internet at http://pubs.acs.org.

## ■ AUTHOR INFORMATION

### Corresponding Author

*E-mail: danny@chem.wisc.edu.

### Notes

The authors declare no competing financial interest.

## ■ ACKNOWLEDGMENTS

This Article is dedicated to the memory of Prof. John Corbett, who showed so many of us how the greatest gift that synthesis offers is not validation of our own preconceived notions but the discovery of new possibilities beyond imagining. We thank Dr. John Fournelle for assistance with the EPMA measurements. We gratefully acknowledge the financial support of the U.S. Department of Energy, Office of Science Early Career Program (Grant DE-SC0003947), through the Office of Basic Energy Sciences. B.J.K. thanks the National Science Foundation for a graduate student fellowship (Grant DGE-1256259). This research involved calculations using computer resources supported by National Science Foundation Grant CHE-0840494.

## ■ REFERENCES

(1) Smithells, C. J.; Gale, W. F.; Totemeier, T. C. *Smithells metals reference book*, 8th ed.; Elsevier Butterworth-Heinemann: Amsterdam, The Netherlands, 2004.
(2) Fredrickson, D. C.; Lee, S.; Hoffmann, R. *Angew. Chem., Int. Ed.* **2007**, *46*, 1958−1976.
(3) Conrad, M.; Harbrecht, B.; Weber, T.; Jung, D. Y.; Steurer, W. *Acta Crystallogr., Sect. B* **2009**, *65*, 318−325.
(4) Weber, T.; Dshemuchadse, J.; Kobas, M.; Conrad, M.; Harbrecht, B.; Steurer, W. *Acta Crystallogr., Sect. B* **2009**, *65*, 308−317.
(5) Guo, Y.; Stacey, T. E.; Fredrickson, D. C. *Inorg. Chem.* **2014**, *53*, 5280−5293.
(6) Harris, N. A.; Hadler, A. B.; Fredrickson, D. C. *Z. Anorg. Allg. Chem.* **2011**, *637*, 1961−1974.
(7) Hadler, A. B.; Harris, N. A.; Fredrickson, D. C. *J. Am. Chem. Soc.* **2013**, *135*, 17369−17378.
(8) Solokha, P.; De Negri, S.; Pavlyuk, V.; Saccone, A. *Solid State Sci.* **2009**, *11*, 801−811.
(9) Kovnir, K.; Shatruk, M. *Eur. J. Inorg. Chem.* **2011**, *2011*, 3955−3962.
(10) Yvon, K. *Acta Crystallogr., Sect. B* **1974**, *30*, 853−861.
(11) Girgis, K.; Petter, W.; Pupp, G. *Acta Crystallogr., Sect. B* **1975**, *31*, 113−116.
(12) Häussermann, U.; Viklund, P.; Svensson, C.; Eriksson, S.; Berastegui, P.; Lidin, S. *Angew. Chem., Int. Ed.* **1999**, *38*, 488−492.
(13) Yvon, K. *Acta Crystallogr., Sect. B* **1975**, *31*, 117−120.
(14) Okamoto, H. In *Binary Alloy Phase Diagrams*, 2nd ed.; Massalski, T. B., Ed.; ASM International: Materials Park, OH, 1990; Vol. 2, pp 1861−1862.
(15) Baron, V. V.; Myzenkova, L. F.; Savitskii, E. M.; Gladyshevskii, E. I. *Zh. Neorg. Khim.* **1964**, *9*, 2170−2173.

(16) Carrillo-Cabrera, W.; Caroca-Canales, N.; von Schnering, H. G. *Z. Anorg. Allg. Chem.* **1994**, *620*, 247−257.
(17) Flot, D.; Tillard-Charbonnel, M.; Belin, C. *New J. Chem.* **1998**, *22*, 591−598.
(18) Blatov, V. A.; Shevchenko, A. P.; Proserpio, D. M. *Cryst. Growth Des.* **2014**, *14*, 3576−3586.
(19) Heusler, O. *Ann. Phys.-Berlin* **1934**, *411*, 155−201.
(20) Such a hierarchical relationship to the $MnAlCu_2$ type has also been noted for the $Tb_{117}Fe_{52}Ge_{112}$ type. See ref 9.
(21) Yannello, V. J.; Kilduff, B. J.; Fredrickson, D. C. *Inorg. Chem.* **2014**, *53*, 2730−2741.
(22) Girgis, K. *J. Cryst. Growth* **1975**, *30*, 99−100.
(23) Oszlányi, G.; Sütő, A. *Acta Crystallogr., Sect. A* **2004**, *60*, 134−141.
(24) Oszlányi, G.; Sütő, A. *Acta Crystallogr., Sect. A* **2005**, *61*, 147−152.
(25) Palatinus, L.; Chapuis, G. *J. Appl. Crystallogr.* **2007**, *40*, 786−790.
(26) Petříček, V.; Dušek, M.; Palatinus, L. *Z. Kristallogr.* **2014**, *229*, 345−352.
(27) Momma, K.; Izumi, F. *J. Appl. Crystallogr.* **2011**, *44*, 1272−1276.
(28) Donovan, J. J.; Kremswer, D.; Fournelle, J.; Karsten, G. *Probe for EPMA User's Guide and Reference*; Probe Software, Inc.: Eugene, OR, 2013.
(29) Kresse, G.; Furthmüller, J. *Phys. Rev. B* **1996**, *54*, 11169−11186.
(30) Kresse, G.; Furthmüller, J. *Comput. Mater. Sci.* **1996**, *6*, 15−50.
(31) Vanderbilt, D. *Phys. Rev. B* **1990**, *41*, 7892−7895.
(32) Stacey, T. E.; Fredrickson, D. C. *Dalton Trans.* **2012**, *41*, 7801−7813.
(33) Landrum, G. A.; Glassey, W. V. *YAeHMOP*: Yet Another extended Hückel Molecular Orbital Package. *YAeHMOP* is freely available at http://sourceforge.net/projects/yaehmop/. Last accessed: Aug 31, 2014.
(34) In our discussion of the $Ta_4Ga_5$ structure, we treat the filling pattern of the voids of the primitive cubic network of $Ta@Ta_8Ga_6$ units as perfectly ordered. The $Ta_4Ga_5$ and $Ta_{3.9}Mo_{0.1}Ga_5$ crystals that we have examined indicate that this is a slight approximation. Fourier difference maps for this ordered model show noticeable peaks that correspond to some of the Ta positions that would arise when replacing one occupant type with the other. These are listed as Ta8 and Ta9 in Table 2. Occupation of the Ta8 sites leads to the completion of a Ta pentagonal dodecahedron surrounding the voids containing the bcc fragment dimers. The Ta9 site, meanwhile, corresponds to the placement of a pair of Ta atoms (as occurs at the centers of the bcc fragment dimers) into the center of the distorted $Ga_{12}$ icosahedra. These sites exhibit unrealistically short distances to some of the Ga sites (Ga4, Ga8, and Ga9), whose occupancies were thus constrained to a model in which these Ga sites are vacant when their nearby Ta8 or Ta9 sites is occupied. It is likely that the occupation of Ta8 and Ta9 occurs concomitantly with full cluster substitution. However, because of the small values of their refined occupancies (<2%), any remaining disorder has at most a faint signature in the Fourier electron density.
(35) Dryś, M. *J. Less Common Met.* **1978**, *58*, 111−113.
(36) The surface in Figure 7 was generated by placing exponential decay functions of the form $\pm e^{-\zeta r}$ on each of the atomic centers, where $\zeta$ is an adjustable parameter and the positive and negative signs are used for Ta and Ga, respectively. The interface between Ta and Ga domains then emerges when a function $f(x,y,z)$ is constructed from the sums of these atom-centered functions, and the $f = 0$ isosurface is plotted. For the surface in Figure 7, $\zeta$ was set to 2.0 $Å^{-1}$.
(37) Zintl, E.; Dullenkopf, W. *Z. Phys. Chem. B* **1932**, *16*, 195−205.
(38) von Schnering, H. G.; Nesper, R. *Angew. Chem., Int. Ed.* **1987**, *26*, 1059−1080.
(39) Hyde, S.; Andersson, S.; Larsson, K.; Blum, Z.; Landh, T.; Lidin, S.; Ninham, B. W. *The Language of Shape*; Elsevier: Amsterdam, The Netherlands, 1997.
(40) Hyde, S. T.; Andersson, S. *Z. Kristallogr.* **1984**, *168*, 221−254.
(41) Hyde, S. T.; Andersson, S. *Z. Kristallogr.* **1985**, *170*, 225−239.
(42) Dronskowski, R.; Blöchl, P. E. *J. Phys. Chem.* **1993**, *97*, 8617−8624.
(43) Fredrickson, R. T.; Fredrickson, D. C. *Inorg. Chem.* **2012**, *51*, 10341−10349.
(44) Fredrickson, R. T.; Fredrickson, D. C. *Inorg. Chem.* **2013**, *52*, 3178−3189.
(45) Gourdon, O.; Miller, G. J. *J. Solid State Chem.* **2003**, *173*, 137−147.